Supplement of Partitioning anthropogenic and natural methane emissions in Finland during 2000–2021 by combining bottom-up and top-down estimates

Maria K. Tenkanen[1], Aki Tsuruta[1], Hugo Denier van der Gon[2], Lena Höglund-Isaksson[3], Antti Leppänen[1,4], Tiina Markkanen[1], Ana Maria Roxana Petrescu[5], Maarit Raivonen[4], and Tuula Aalto[1]

[1]Climate Research, Finnish Meteorological Institute, 00560 Helsinki, Finland
[2]Department of Air Quality and Emissions Research, TNO, 3584 CB Utrecht, the Netherlands
[3]International Institute for Applied Systems Analysis (IIASA), 2361 Laxenburg, Austria
[4]Institute for Atmospheric and Earth System Research/Physics, Faculty of Science, University of Helsinki, 00014 Helsinki, Finland
[5]Department of Earth Sciences, Vrije Universiteit Amsterdam, 1081HV, Amsterdam, the Netherlands

Correspondence: Maria K. Tenkanen (maria.tenkanen@fmi.fi)

Table S1. Continuation to the Table 1 "List of inversion setups".

Inversion	Termite prior	Ocean prior	Other priors	Atmospheric sink
$Inv_{JSBACH\_CAMSREG}$	VISIT	Tsuruta et al. (2017)		ECHAM5/MESSy1
$Inv_{LPX\_CAMSREG}$	VISIT	Tsuruta et al. (2017)		ECHAM5/MESSy1
Inv_{LPX_EDGAR}	VISIT	Weber et al. (2019)		ECHAM5/MESSy1
$Inv_{LPX\_EDGAR\_UNC}$	VISIT	Weber et al. (2019)		ECHAM5/MESSy1
Inv_{GCP_EDGAR}	Saunois et al. (2020)	Weber et al. (2019)	Geological: Etiope et al. (2019)	Brühl and Crutzen (1993)

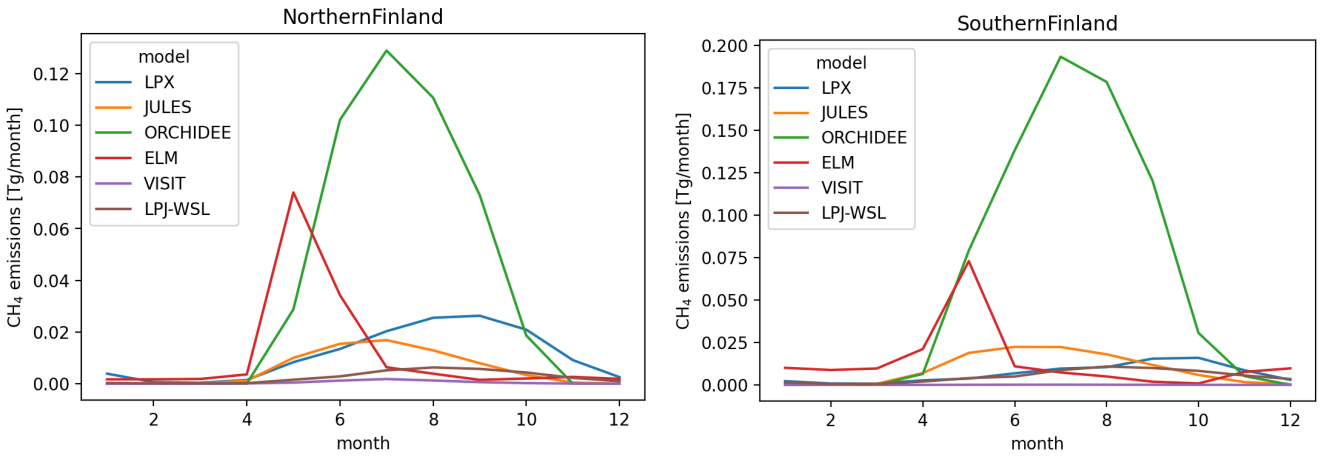

Figure S1. Average monthly CH_4 emissions of process-based models from Saunois et al. (2020) in a) northern and b) southern Finland.

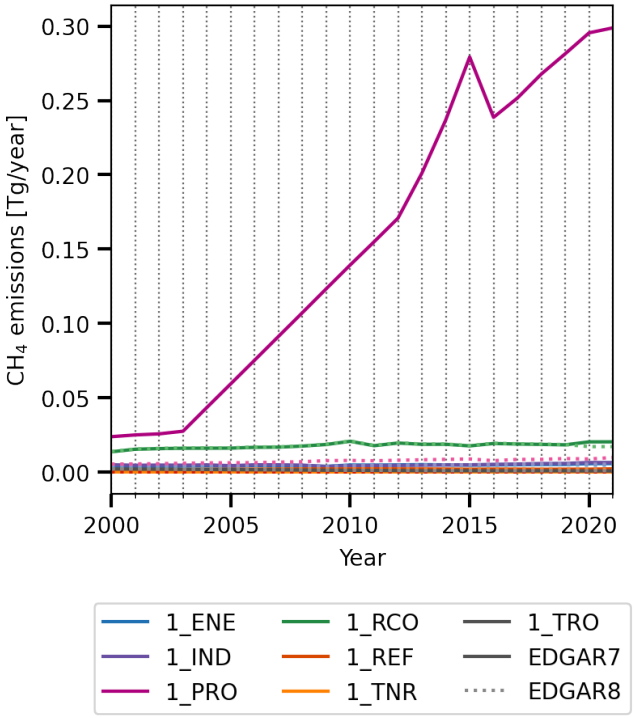

Figure S2. Annual energy sector CH_4 emissions by its components from EDGAR v7 (solid line) and v8 (dotted line).

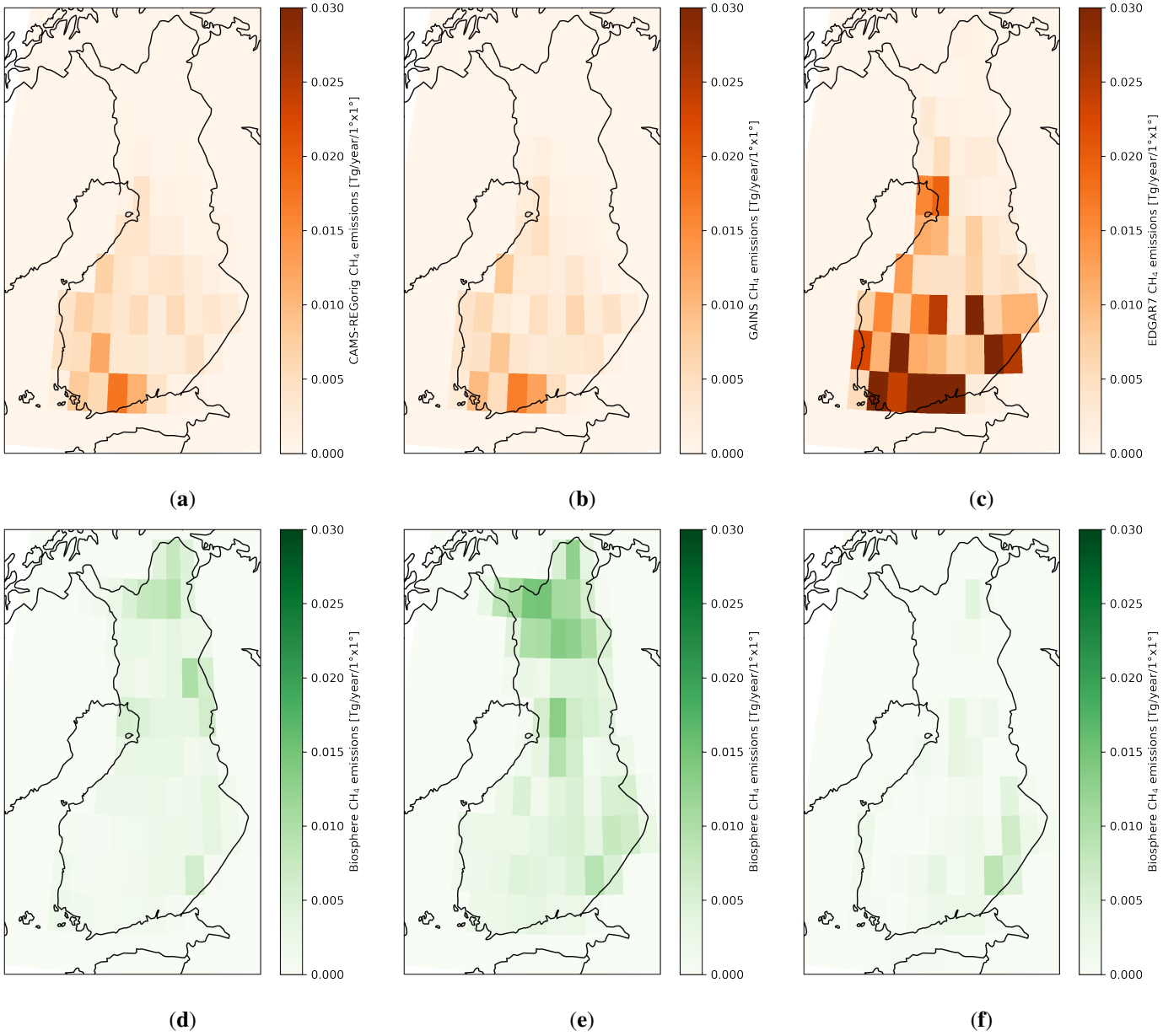

Figure S3. Average annual CH_4 emissions from 2010–2020 of (**a**) CAMS-REG (orig), (**b**) GAINS, (**c**) EDGAR v7, (**d**) LPX-Bern DYPTOP, (**e**) JSBACH-HIMMELI and **f**) GCP biospheric prior.

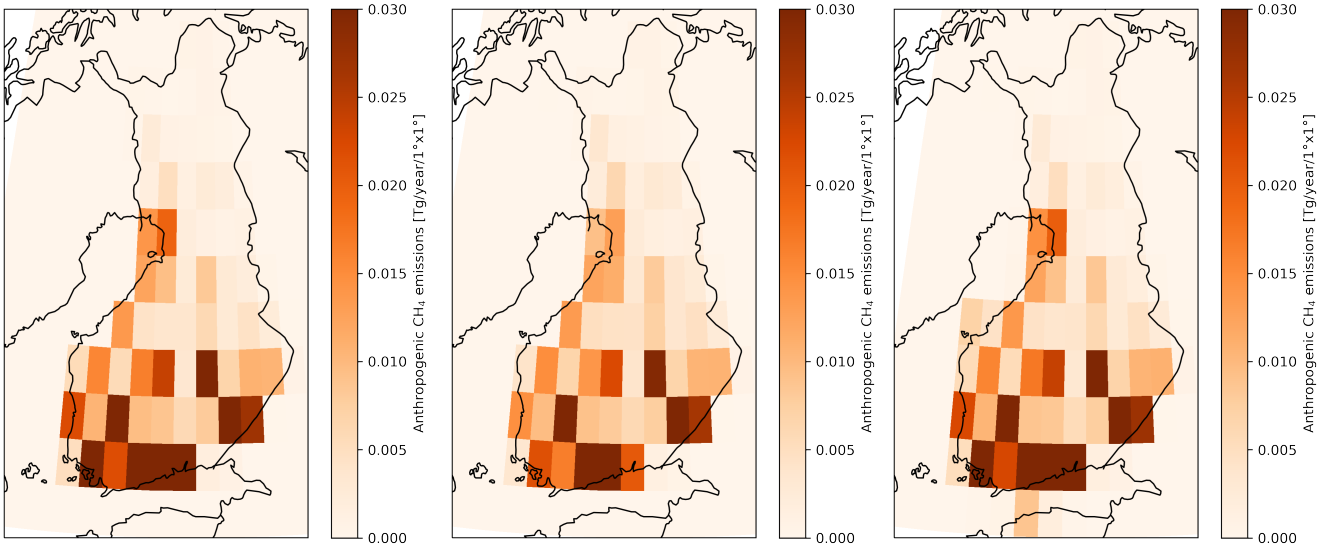

(a) $\text{Inv}_{\text{LPX\_EDGAR}}$ (b) $\text{Inv}_{\text{LPX\_EDGAR\_UNC}}$ (c) $\text{Inv}_{\text{GCP\_EDGAR}}$

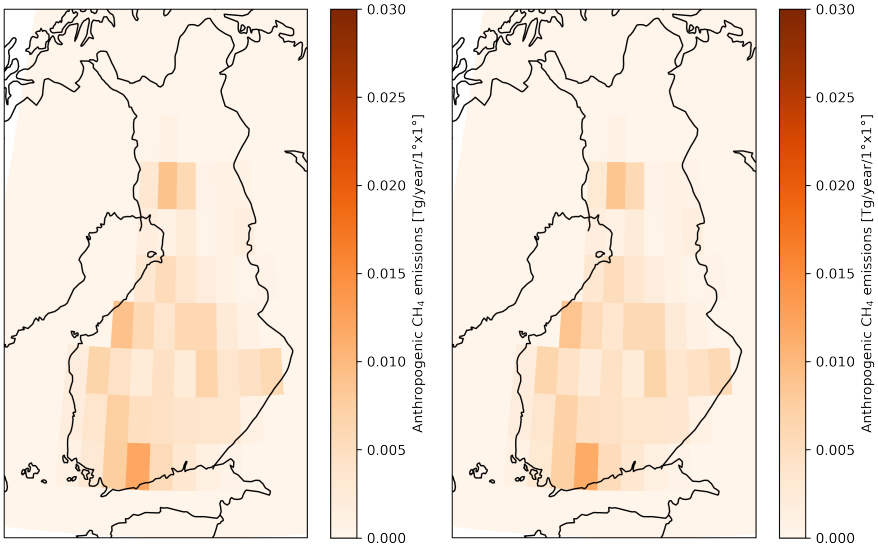

(d) $\text{Inv}_{\text{LPX\_CAMSREG}}$ (e) $\text{Inv}_{\text{JSBACH\_CAMSREG}}$

Figure S4. Average optimised annual anthropogenic CH_4 emissions from 2010–2020 from (**a**) $\text{Inv}_{\text{LPX\_EDGAR}}$, (**b**) $\text{Inv}_{\text{LPX\_EDGAR\_UNC}}$, (**c**) $\text{Inv}_{\text{GCP\_EDGAR}}$, (**d**) $\text{Inv}_{\text{LPX\_CAMSREG}}$ and (**e**) $\text{Inv}_{\text{JSBACH\_CAMSREG}}$

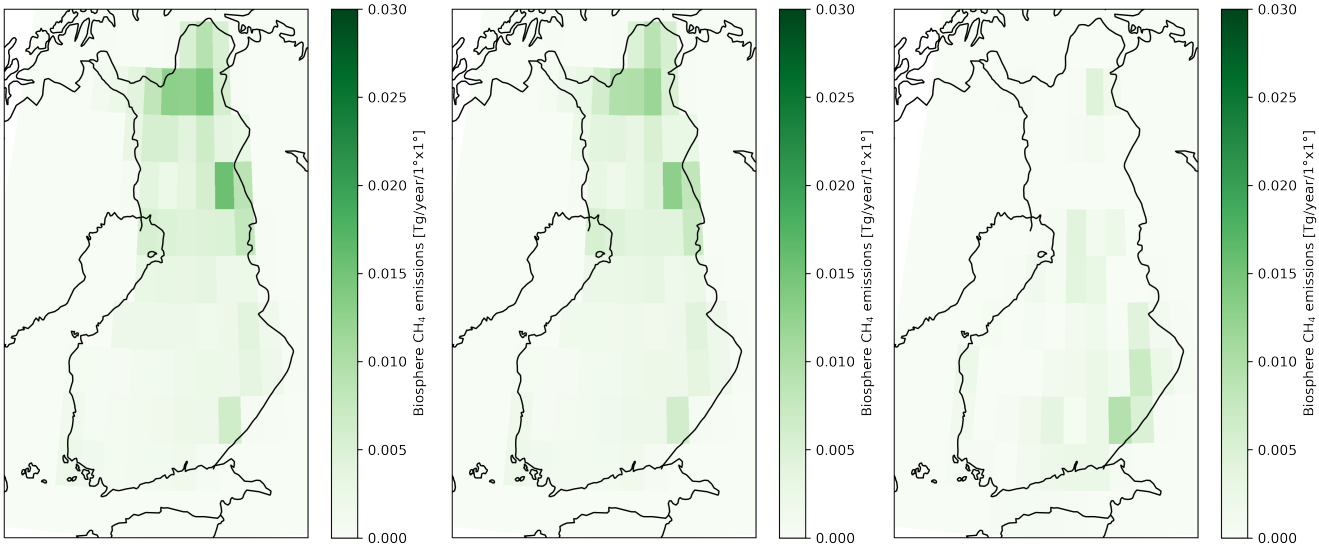

(a) $\text{Inv}_{\text{LPX\_EDGAR}}$ (b) $\text{Inv}_{\text{LPX\_EDGAR\_UNC}}$ (c) $\text{Inv}_{\text{GCP\_EDGAR}}$

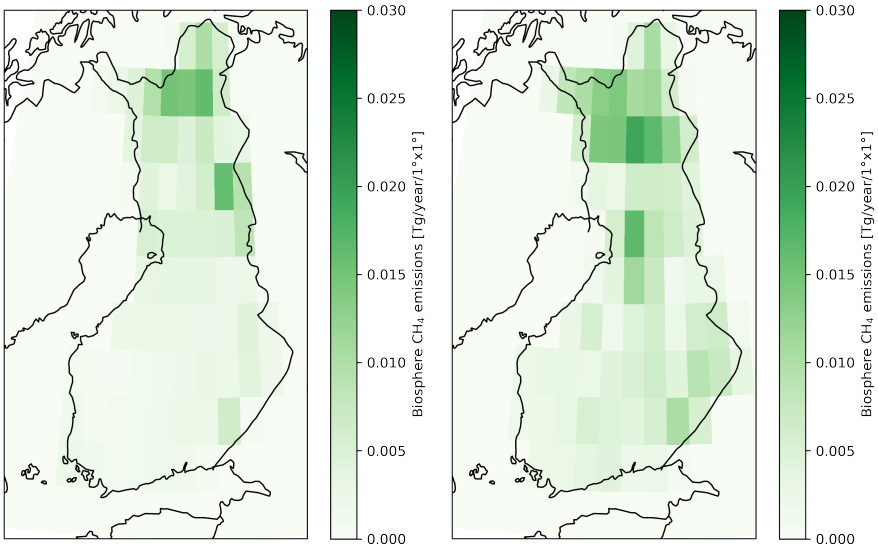

(d) $\text{Inv}_{\text{LPX\_CAMSREG}}$ (e) $\text{Inv}_{\text{JSBACH\_CAMSREG}}$

Figure S5. Average optimised annual natural CH_4 emissions from 2010–2020 from (**a**) $\text{Inv}_{\text{LPX\_EDGAR}}$, (**b**) $\text{Inv}_{\text{LPX\_EDGAR\_UNC}}$, (**c**) $\text{Inv}_{\text{GCP\_EDGAR}}$, (**d**) $\text{Inv}_{\text{LPX\_CAMSREG}}$ and (**e**) $\text{Inv}_{\text{JSBACH\_CAMSREG}}$

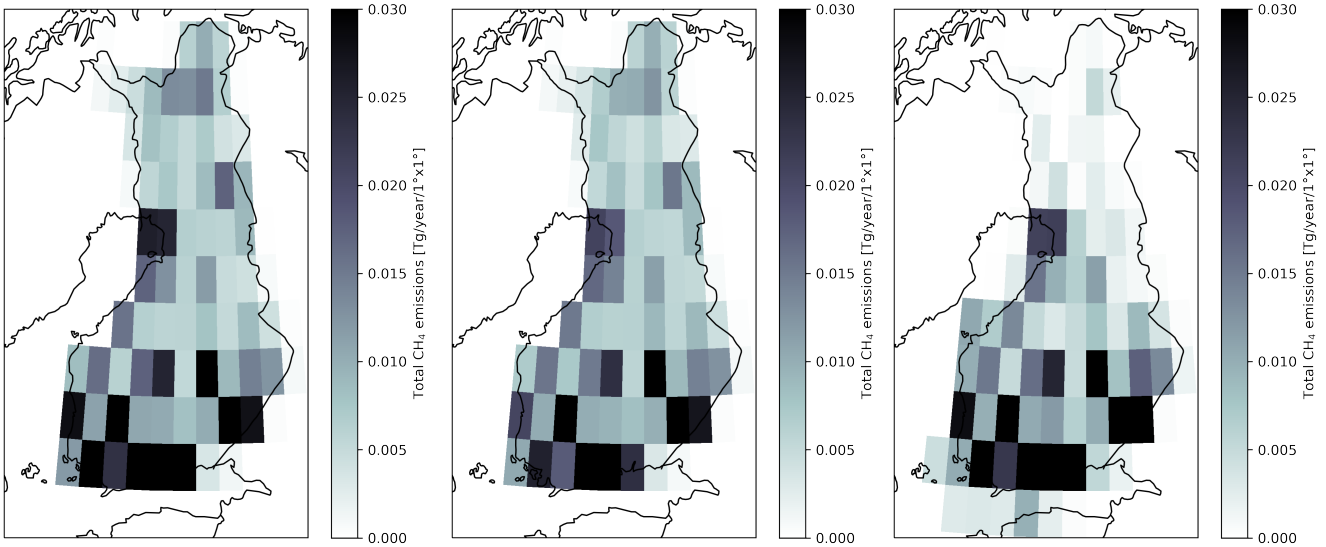

(a) $\text{Inv}_{\text{LPX\_EDGAR}}$ (b) $\text{Inv}_{\text{LPX\_EDGAR\_UNC}}$ (c) $\text{Inv}_{\text{GCP\_EDGAR}}$

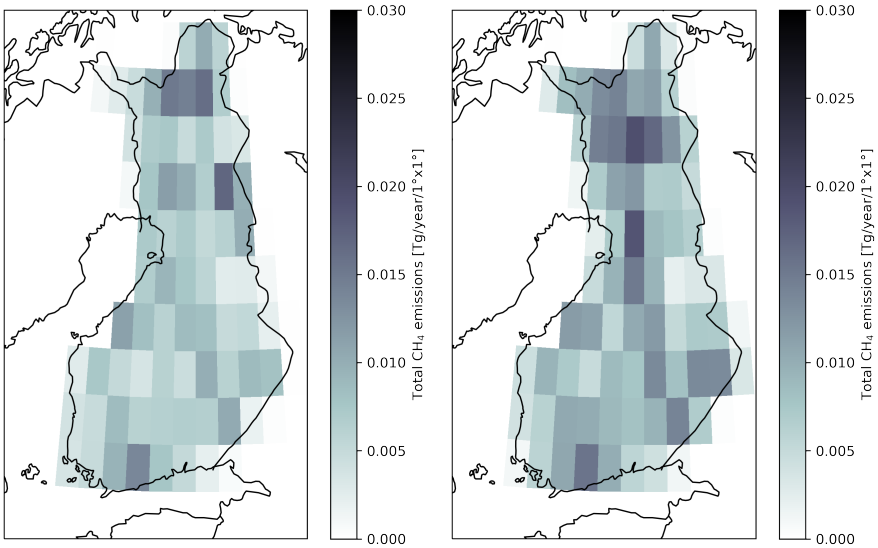

(d) $\text{Inv}_{\text{LPX\_CAMSREG}}$ (e) $\text{Inv}_{\text{JSBACH\_CAMSREG}}$

Figure S6. Average optimised annual total CH_4 emissions from 2010–2020 from (**a**) $\text{Inv}_{\text{LPX\_EDGAR}}$, (**b**) $\text{Inv}_{\text{LPX\_EDGAR\_UNC}}$, (**c**) $\text{Inv}_{\text{GCP\_EDGAR}}$, (**d**) $\text{Inv}_{\text{LPX\_CAMSREG}}$ and (**e**) $\text{Inv}_{\text{JSBACH\_CAMSREG}}$

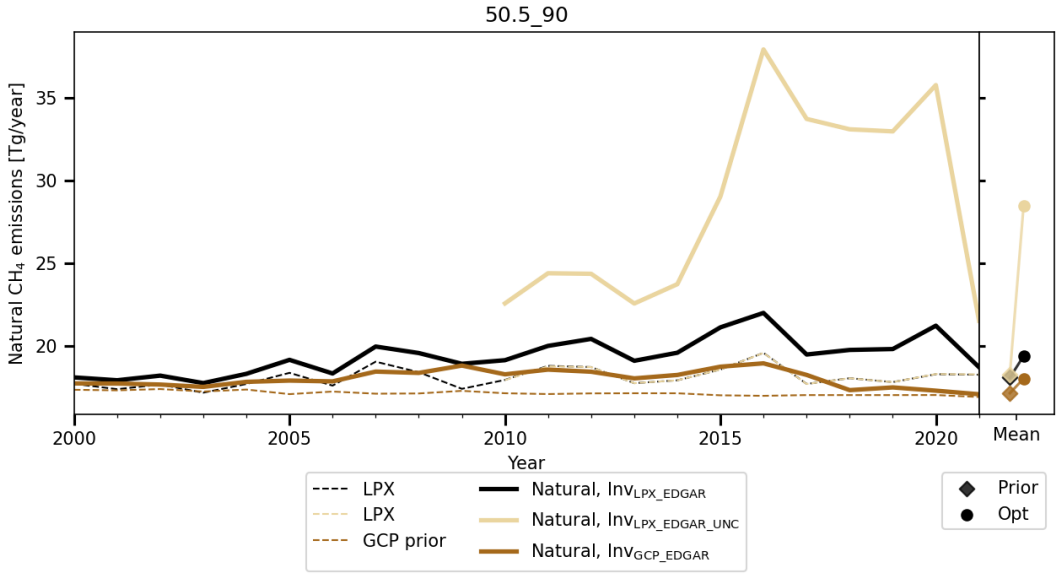

Figure S7. Annual natural CH_4 emission estimates from three CTE-CH_4 inversion model runs in latitudes northern than 50° N. Prior estimates are shown with dashed and optimised estimates with solid lines. The right panel shows the mean prior and optimised estimates from the whole study period.

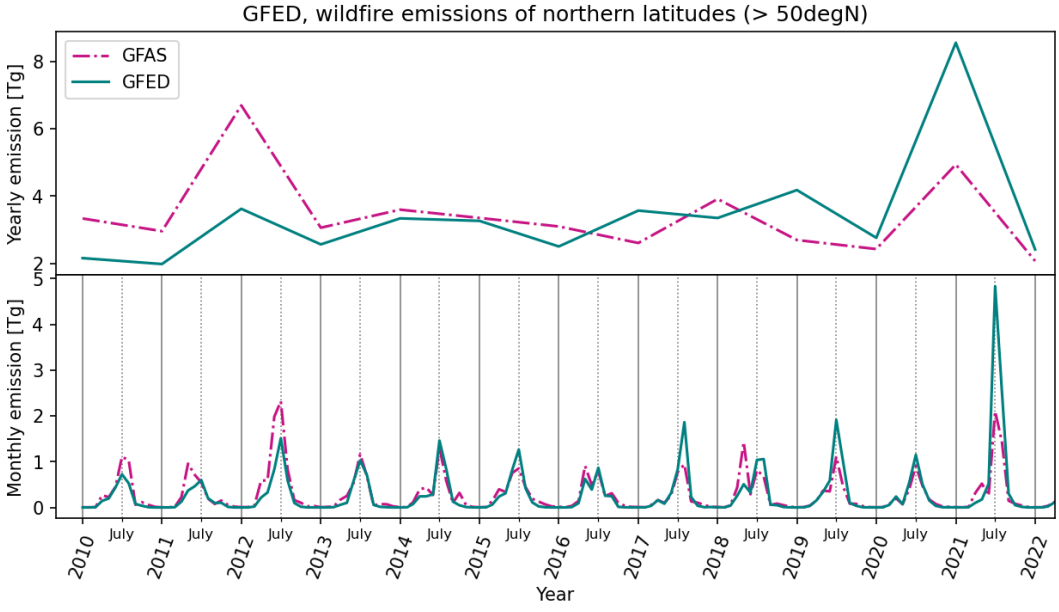

Figure S8. Annual (top) and monthly (bottom) CH_4 emissions from GFAS (dashed line) and GFED (solid line) in latitudes northern than 50° N.

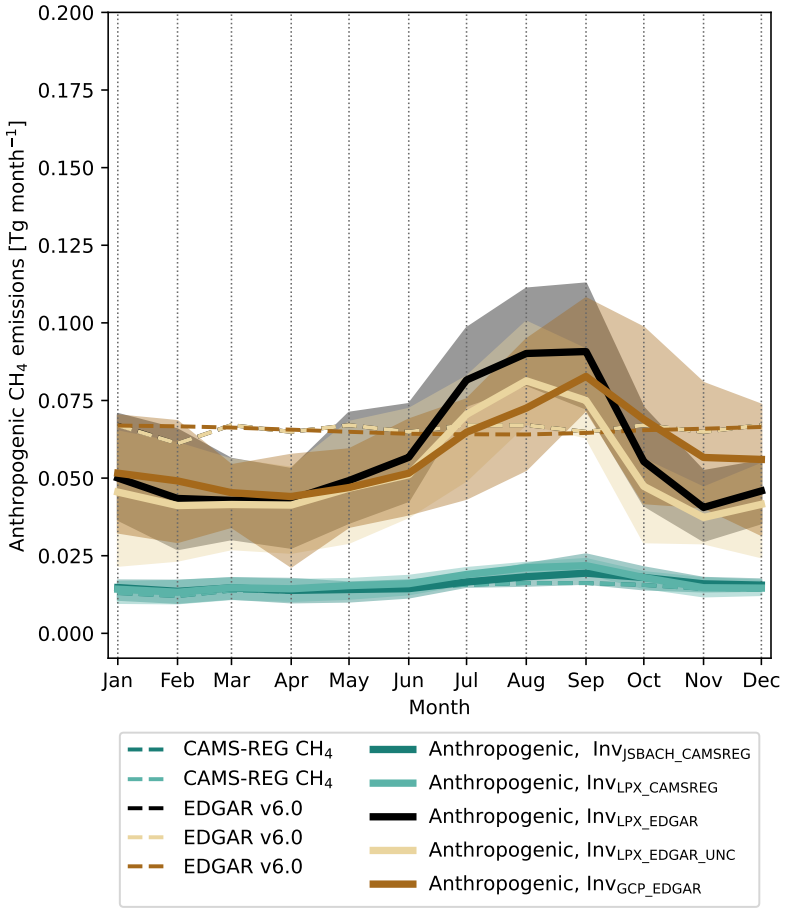

Figure S9. Average monthly anthropogenic CH_4 emission estimates from the five CTE-CH_4 inversion model runs in Finland in 2010–2020. Prior estimates are shown with dashed and optimised estimates with solid lines. The shaded areas show the smallest and the largest monthly posterior emission estimates.

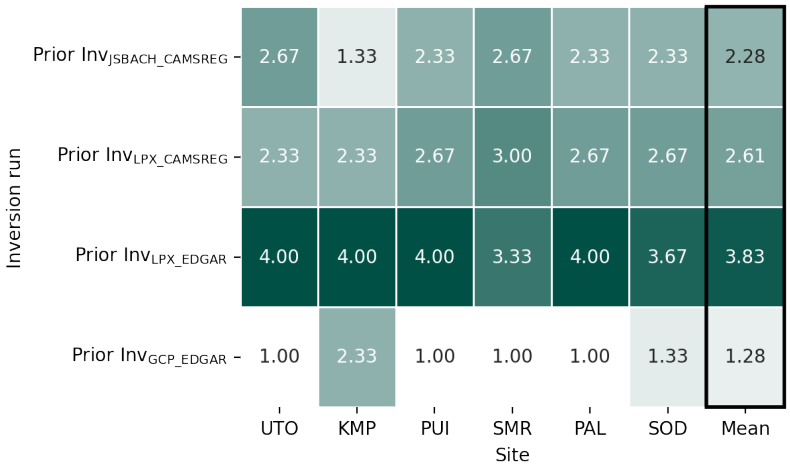

Figure S10. The average rank calculated for each site for each forward run (with prior emissions) is shown. The bias, the detrended RMSE and the detrended R were calculated with each forward run in each site and values were then ranked between the model estimates (the smallest being the best with bias and RMSE and the highest being the best with R). Additionally, the right-most column is the average over all sites averages.

References

Brühl, C. and Crutzen, P. J.: MPIC two-dimensional model, Tech. rep., NASA, Washington, DC, 1993.

Etiope, G., Ciotoli, G., Schwietzke, S., and Schoell, M.: Gridded maps of geological methane emissions and their isotopic signature, Earth System Science Data, 11, 1–22, https://doi.org/10.5194/essd-11-1-2019, 2019.

Saunois, M., Stavert, A. R., Poulter, B., Bousquet, P., Canadell, J. G., Jackson, R. B., Raymond, P. A., Dlugokencky, E. J., Houweling, S., Patra, P. K., Ciais, P., Arora, V. K., Bastviken, D., Bergamaschi, P., Blake, D. R., Brailsford, G., Bruhwiler, L., Carlson, K. M., Carrol, M., Castaldi, S., Chandra, N., Crevoisier, C., Crill, P. M., Covey, K., Curry, C. L., Etiope, G., Frankenberg, C., Gedney, N., Hegglin, M. I., Höglund-Isaksson, L., Hugelius, G., Ishizawa, M., Ito, A., Janssens-Maenhout, G., Jensen, K. M., Joos, F., Kleinen, T., Krummel, P. B., Langenfelds, R. L., Laruelle, G. G., Liu, L., Machida, T., Maksyutov, S., McDonald, K. C., McNorton, J., Miller, P. A., Melton, J. R., Morino, I., Müller, J., Murguia-Flores, F., Naik, V., Niwa, Y., Noce, S., O'Doherty, S., Parker, R. J., Peng, C., Peng, S., Peters, G. P., Prigent, C., Prinn, R., Ramonet, M., Regnier, P., Riley, W. J., Rosentreter, J. A., Segers, A., Simpson, I. J., Shi, H., Smith, S. J., Steele, L. P., Thornton, B. F., Tian, H., Tohjima, Y., Tubiello, F. N., Tsuruta, A., Viovy, N., Voulgarakis, A., Weber, T. S., van Weele, M., van der Werf, G. R., Weiss, R. F., Worthy, D., Wunch, D., Yin, Y., Yoshida, Y., Zhang, W., Zhang, Z., Zhao, Y., Zheng, B., Zhu, Q., Zhu, Q., and Zhuang, Q.: The Global Methane Budget 2000–2017, Earth System Science Data, 12, 1561–1623, https://doi.org/10.5194/essd-12-1561-2020, 2020.

Tsuruta, A., Aalto, T., Backman, L., Hakkarainen, J., van der Laan-Luijkx, I. T., Krol, M. C., Spahni, R., Houweling, S., Laine, M., Dlugokencky, E., Gomez-Pelaez, A. J., van der Schoot, M., Langenfelds, R., Ellul, R., Arduini, J., Apadula, F., Gerbig, C., Feist, D. G., Kivi, R., Yoshida, Y., and Peters, W.: Global methane emission estimates for 2000–2012 from CarbonTracker Europe-CH4 v1.0, Geoscientific Model Development, 10, 1261–1289, https://doi.org/10.5194/gmd-10-1261-2017, 2017.

Weber, T., Wiseman, N. A., and Kock, A.: Global ocean methane emissions dominated by shallow coastal waters, Nature Communications, 10, 4584, https://doi.org/10.1038/s41467-019-12541-7, 2019.